



HAL
open science

Reactive uptake of NO₂ on volcanic particles: A possible source of HONO in the atmosphere

Manolis Romanias, Yangang Ren, Benoit Grosselin, Véronique Daële, Abdelwahid S Mellouki, Pavla Dagsson-Waldhauserova, Frédéric Thévenet

► To cite this version:

Manolis Romanias, Yangang Ren, Benoit Grosselin, Véronique Daële, Abdelwahid S Mellouki, et al.. Reactive uptake of NO₂ on volcanic particles: A possible source of HONO in the atmosphere. *Journal of Environmental Sciences*, 2020, 95, pp.155-164. 10.1016/j.jes.2020.03.042 . hal-02909300

HAL Id: hal-02909300

<https://hal.science/hal-02909300v1>

Submitted on 26 Dec 2020

HAL is a multi-disciplinary open access archive for the deposit and dissemination of scientific research documents, whether they are published or not. The documents may come from teaching and research institutions in France or abroad, or from public or private research centers.

L'archive ouverte pluridisciplinaire **HAL**, est destinée au dépôt et à la diffusion de documents scientifiques de niveau recherche, publiés ou non, émanant des établissements d'enseignement et de recherche français ou étrangers, des laboratoires publics ou privés.

1 **Reactive uptake of NO₂ on volcanic particles: a possible source of HONO in the**
2 **atmosphere**

3

4 Manolis N Romanias^{1,*}, Yangang Ren², Benoit Grosselin², Véronique Daële², Abdelwahid
5 Mellouki², Pavla Dagsson-Waldhauserova^{3,4}, Frederic Thevenet¹

6 1. IMT Lille Douai, Univ. Lille, SAGE, F-59000 Lille, France

7 2. CNRS-ICARE/OSUC, 45071, Orléans, France

8 3. Agricultural University of Iceland, Keldnaholt, Reykjavik 112, Iceland

9 4. Faculty of Environmental Sciences, Czech University of Life Sciences, Prague 165 21,
10 Czech Republic

11

12

13

14 * Corresponding author. E-mail: emmanouil.romanias@imt-lille-douai.fr (Manolis N
15 Romanias)

16

Abstract

17
18 The heterogeneous degradation of nitrogen dioxide (NO_2) on five samples of natural Icelandic
19 volcanic particles has been investigated. Laboratory experiments were carried out under simulated
20 atmospheric conditions using a coated wall flow tube (CWFT). The CWFT reactor was coupled to a
21 blue light nitrogen oxides analyzer (NO_x analyzer), and a long path absorption photometer (LOPAP) to
22 monitor in real time the concentrations of NO_2 , NO and HONO respectively. Under dark and ambient
23 relative humidity conditions, the steady state uptake coefficients of NO_2 varied significantly between
24 the volcanic samples probably due to differences in magma composition and morphological variation
25 related with the density of surface OH groups. The irradiation of the surface with simulated sunlight
26 enhanced the uptake coefficients by a factor of three indicating that photo-induced processes on the
27 surface of the dust occur. Furthermore, the product yields of NO and HONO were determined under
28 both dark and simulated sunlight conditions. The relative humidity was found to influence the
29 distribution of gaseous products, promoting the formation of gaseous HONO. A detailed reaction
30 mechanism is proposed that supports our experimental observations. Regarding the atmospheric
31 implications, our results suggest that the NO_2 degradation on volcanic particles and the corresponding
32 formation of HONO is expected to be significant during volcanic dust storms or after a volcanic
33 eruption.

34 **Keywords:**

35 volcanic dust

36 HONO

37 Uptake coefficients

38 Product yields

39 Simulated atmospheric conditions

1. Introduction

40 Nitrogen dioxide (NO_2) is an important atmospheric pollutant that contributes to the formation of
41 photochemical smog, (von Schneidmesser et al., 2015). NO_2 acts as an intermediate species in several
42 gas phase photochemical cycles occurring in the troposphere affecting the radical budgets for
43 hydroperoxyl radicals (HO_x) and Peroxy radicals (RO_x), as well as that of ozone (O_3). In addition, the
44 chemistry of NO_2 is involved in the formation of organic nitrates (Nault et al., 2016; Perring et al.,
45 2013; von Schneidmesser et al., 2015). Besides gas phase chemistry, the heterogeneous reactivity of
46 NO_2 with atmospheric particles has been shown to play an important role in atmospheric processes.
47 NO_2 reacts with aerosols forming nitrous acid (HONO), a key atmospheric species, precursor of the
48 major atmospheric oxidant: OH radicals (Mellouki et al., 2015). So far, atmospheric simulation
49 models fail to reproduce the unexpectedly high daytime concentrations of HONO reported in field
50 campaigns, suggesting the existence of new, yet unknown, sources of HONO (Kleffmann, 2007;
51 Romer et al., 2018). Therefore, it has been suggested that the heterogeneous conversion of NO_2 to
52 HONO could possibly explain the discrepancies between atmospheric models and field observations
53 (Romer et al., 2018).

55 The heterogeneous reaction of NO_2 on various type of atmospheric particles, e.g. salts, soot, mineral
56 dust and proxies, has been already reported in literature (Crowley et al., 2010; George et al., 2015;
57 Tang et al., 2017). However, the interaction of NO_2 with volcanic particles under simulated
58 atmospheric conditions has not been studied. Actually, the role of volcanic aerosols on tropospheric
59 chemistry has not been thoroughly evaluated yet. Volcanic aerosols may act as platforms for the
60 scavenging or conversion of key atmospheric species (e.g. NO_2 , O_3 , SO_2 etc.), and thus, impact the
61 tropospheric oxidation capacity regionally, or in a larger scale such as during massive volcanic
62 eruptions or during extreme dust storms of volcanic dust as reported for instance in Iceland (Arnalds et
63 al., 2016; Arnalds et al., 2013; Moroni et al., 2018; Ovadnevaite et al., 2009).

64 Considering that nearly 10% of the world population is living in the vicinity of active volcanos (Auker
65 et al., 2013), it is expected that pollutants emitted from anthropogenic sources, such as nitrogen oxide
66 species (NO_x), O_3 etc. can interact or react with naturally emitted volcanic gases or volcanic aerosols.

67 A prime example is Mexico City, known as one of the most polluted city in the world, situated 70 km
68 away from the frequently erupting Popocatepetl volcano. Besides, distal urban environments can also
69 be impacted by volcanic pollution. Resuspension of volcanic ash, defined as volcanic dust, or v-dust,
70 for the following of the paper, can prolong the effects of volcanic eruptions several months after the
71 eruption is finished (Arnalds et al., 2013; Butwin et al., 2019; Wilson et al., 2011). The recent
72 eruptions of Icelandic volcanoes Eyjafjallajökull (2010) and Grimsvötn (2011) resulted in the dispersal
73 of massive loads of ashes and aerosols over a large part of Europe and Northern Atlantic
74 (Gudmundsson et al., 2012; Ilyinskaya et al., 2017). Holuhraun (2014-2015) was an effusive eruption
75 occurring in the center of volcanic dust hot spot, but volcanic dust was frequently suspended during
76 the eruption (Pfeffer et al., 2018; Vignelles et al., 2016). Therefore, volcanic aerosols are regularly
77 emitted in the atmosphere and recent studies have shown that their lifetime is significantly longer than
78 it has been estimated (Boichu et al., 2016).

79 Consequently, the objective of the current study is to determine experimentally how efficiently NO₂ is
80 scavenged on volcanic particles and to evaluate whether this interaction can be a significant source of
81 HONO in the atmosphere - on local or regional scale - during severe volcanic dust storms or volcanic
82 eruptions. To that end, laboratory experiments have been carried out under simulated atmospheric
83 conditions (temperature, relative humidity, NO₂ concentrations and simulated sunlight radiation)
84 employing a flow tube coupled with state of the art instrumentation for the simultaneous detection of
85 NO₂, NO and HONO. The reactive uptake coefficients of NO₂ are measured and the yields of the
86 products formed, and the mechanism of the reaction are addressed.

87 **2. Materials and methods**

88

89 **2.1 Materials**

90 **2.1.1 Origin of the volcanic samples**

91 In the current paper, Iceland was chosen as a case study. Iceland is a very active geological site of
92 Earth with more than 30 active volcanoes and large eruptions occurring every 3 to 5 years. Hence it is
93 considered as the largest volcanic desert on Earth (Arnalds et al., 2016) with estimated dust deposition

94 of 31 - 40 million tons per year (Arnalds et al., 2014), that could represents up to 7% of total global
95 dust emissions and up to 21% of the Saharan dust emissions (Arnalds et al., 2014; Engelstaedter et al.,
96 2006). Remote sensing studies have evidenced that volcanic plumes formed after a volcanic eruption
97 in Iceland can travel thousands of kilometers impacting urban populated areas of northern Europe
98 (Boichu et al., 2016). Moreover, Iceland is one of the most active aeolian areas on the planet, where
99 unstable sandy surfaces are widespread and are subjected to frequent high-velocity winds, resulting in
100 numerous wind erosion events and massive volcanic dust storms (Arnalds et al., 2016). In Iceland,
101 around 100 dust events are reported each year (Arnalds et al., 2014); up to 300,000 tons of dust can be
102 emitted in a single storm. Particulate matter 10 micrometers or less in diameter (i.e. PM₁₀) mass
103 concentrations during dust storms can exceed 7000 µg/m³ with a 1000 µg/m³ 24-h average
104 concentration (Dagsson-Waldhauserova et al., 2015; Thorsteinsson et al., 2011) striking populated
105 areas such as Reykjavik (Dagsson-Waldhauserova et al., 2016). Satellite images confirm that during a
106 dust storm, v-dust particles can travel distances longer than 1000 km impacting the air quality of
107 central Greenland and northern Europe (Arnalds et al., 2016). In a recent study (Đorđević et al., 2019)
108 it has been shown that volcanic dust from Iceland can be transported to even central Balkans, and
109 authors pointed at the fact that Icelandic dust can contribute to impaired air quality in mainland
110 Europe. Icelandic dust is also transported towards Arctic (Groot Zwaafink et al., 2017; Moroni et al.,
111 2018).

112 The volcanic samples investigated in the present work were collected from different desert regions of
113 Iceland, so called dust hot spots Hagavatn, Mýrdalssandur, Maelifellssandur and Dyngjusandur, while
114 the fifth sample of Eyjafjallajökull volcanic ash, named typical ash in the following of the article, was
115 collected several hours after the eruption of the Eyjafjallajökull in 2010 (Gislason et al., 2011).
116 Details about the characterization of the physical and chemical properties of the samples can be found
117 elsewhere (Baratoux et al., 2011; Dagsson-Waldhauserova et al., 2014b; Moroni et al., 2018; Urupina
118 et al., 2019) and for clarity are briefly discussed in Appendix A. Supplementary data.

119 2.1.2 Gases

120 The laboratory experiments were carried out using dry zero air as bath gas (moisture level ca. 2 ppmV)
121 inside a photochemical flow tube. For experiments requiring humid air, an extra flow of zero air
122 passing through a bubbler containing ultrapure water (milli-Q, resistivity 18.2 M Ω -cm) was mixed
123 with the dry air flow, in proportions required to reach the targeted relative humidity (RH). The exact
124 RH in the gas flow is determined and monitored using a temperature and RH probe (KIMO HQ 210,
125 KIMO instruments, United Kingdom). Certified gas cylinders were used as NO₂ source. For low
126 concentration experiments, aiming to determine uptake coefficients in the flow tube, a NO₂ cylinder of
127 200 ppbV in air (Air Liquide, France) was used. As far as concerns the experiments carried out to
128 determine the irradiance intensity inside the flow tube reactor, rather high concentrations of NO₂ were
129 used supplied from a NO₂ cylinder of 50 ppmV in N₂ (Praxair, Belgium).

130 2.1.3 Surface preparation.

131 A few mg of the volcanic sample was placed inside a Pyrex tube (20 cm length, 0.98 cm internal
132 diameter) and, depending on the volcanic sample mass, diluted in 0.5 to 2 mL of water. Then the tube
133 was hand-shaken, so that the water/dust suspension homogeneously spreads on the walls of the tube
134 without any trace of the suspension to be removed after the deposition. Thereafter, the tube was heated
135 at 120°C with a heat-gun for several minutes and further dried overnight in an oven at 100°C. It should
136 be noted that potential modifications of the volcanic dust upon its dissolution in water in the process of
137 slurry preparation and subsequent drying process are expected to be of limited extend (Urupina et al.,
138 2019), and not to influence the uptake coefficients measured in the current study.

139 2.2 Experimental set up

140 The uptake experiments of NO₂ on the volcanic samples were performed using a horizontal
141 double wall Pyrex atmospheric pressure coated wall flow tube reactor (CWFT) (**Fig. 1**). Further details
142 of the experimental set up have been described in previous publications (Lasne et al., 2018; Urupina et
143 al., 2019). The Pyrex tube with the inner coated surface was introduced into the main reactor along its
144 axis. Two Viton O-rings were placed in both ends of the Pyrex tube to set its position. NO₂ was
145 introduced in the reactor by means of a movable injector with internal diameter 0.3 cm. The injector
146 can be moved along the main axis of the coated Pyrex tube, allowing the variation of the v-dust

147 sample length exposed to NO₂ and consequently the contact time (*t*). The total flow rate was regulated
148 between 200 and 400 mL/min, ensuring laminar flow conditions (Reynold number, Re, < 140).

149 The outlet gas flow was then mixed with a dry zero air flow (to compensate the sampling flow of the
150 analytical instruments) and was either sent to a NO_x analyzer (Teledyne T 200UP, Teledyne API,
151 United States) equipped with a blue light converter for the detection of NO₂ (detection limit 50 pptV),
152 and nitrogen oxide (NO that appeared as reaction product), or to a long path absorption photometer
153 (LOPAP, QUMA, Germany) to monitor HONO (reaction product) with a limit of detection of 1-2
154 pptV. Teledyne T 200UP NO_x analyzer uses photolysis in its conversion process; the gas flow passes
155 through a conversion chamber and it is exposed to a blue light from two high powered ultraviolet light
156 emitting diodes (LEDs) characterized by narrow emission bands centered at 395 nm as reported in **Fig.**
157 **2** (bell curve area). The emission band of the LED includes NO₂ absorption band with negligible
158 interferences expected from other gases such as HONO or NO₃ radicals. Consequently, unlike NO_x
159 analyzers relying molybdenum converters, the selective detection of NO₂ is achieved. Based on the
160 LED output intensity and wavelength range as well as the absorption cross section of HONO given in
161 **Fig. 2**, we estimated that the HONO interference to NO₂ concentration to be lower than 3%.

162 To further evaluate possible interferences to NO₂ concentration measured along the uptake
163 experiments, in a dedicated set of experiments a cavity attenuated phase shift (CAPS) NO₂ analyzer
164 (AS32M, ENVEA S.A, France) was additionally coupled with the reactor. The NO₂ CAPS (detection
165 limit 100 pptV) provides a direct absorption measurement of nitrogen dioxide at 450 nm and does not
166 require any conversion of NO₂ to another species. Thus, no interference from other N-containing
167 species are possible. Therefore, comparing the concentrations of NO₂ monitored with the NO_x analyzer
168 and the CAPS we concluded that the possible interference of HONO is around 2% and thus included
169 in our experimental uncertainties.

170 **2.3 Light source characterization.**

171 The CWFT reactor was surrounded by 3 Ultraviolet A lamps (UVA, Philips lighting 18 Watt; 315–400
172 nm with maximum emission at 352 nm) (Romanias et al., 2017). In order to characterize the irradiance
173 intensity in the flow tube, the NO₂ photolysis frequency was measured as a function of the number of

174 lamps turned on. These experiments were carried out with rather high NO₂ concentrations of ca. 10¹⁵
175 molecule/cm³, i.e. 50 ppmV, using dry N₂ as bath gas. NO₂ concentration was monitored with a
176 chemical ionization mass spectrometer (SIFT-MS, Syft Technology, new Zealand) (Romanías et al.,
177 2016; Romanias et al., 2016; Zeineddine et al., 2017). The values of NO₂ photolysis frequency, j_{NO_2}
178 (sec⁻¹), determined from the exponential decays of NO₂ for different numbers of lamps switched on
179 were in the range of 4 to 15 10⁻³ sec⁻¹ (Appendix A **Fig. S2**). Thus it overlaps with the values of J_{NO_2}
180 measured in the atmosphere from cloudy to clear sky conditions (Barnard et al., 2004; Bohn et al.,
181 2005; Topaloglou et al., 2005). Further information regarding the light source characterization
182 experiments are reported in Appendix A. Supplementary data.

183 It has to be noted that under the experimental conditions where the uptake experiments were carried
184 out, the gas phase loss of NO₂ due to its photodissociation is negligible. Indeed, for only 1 UV lamp,
185 i.e. $j_{\text{NO}_2} = 4.5 \times 10^{-3} \text{ sec}^{-1}$, denoted as simulated sunlight conditions in the following of the article, and
186 with a residence time of 2 sec, the gas phase loss of NO₂ due to its photolysis was lower than 0.8%. In
187 case more than one UV lamp was used, the flow in the reactor was increased to maintain gas phase
188 consumption due to photolysis below 1.5% to avoid any impact on the measured uptake coefficient
189 values. To conclude, our experimental measurements of the uptake coefficients and the product yields
190 discussed below are not expected to be biased from interferences or experimental artifacts.

191 **2.4 Uptake of NO₂ on volcanic samples**

192 **2.4.1 Experimental procedure**

193 A typical uptake profile of NO₂ on Hagavavn sample under 30% of RH and 293 K is presented in **Fig.**
194 **3**. It was selected to present breakthrough profiles with all instruments coupled with the flow tube to
195 analyze the outlet flow. In these experiments, the gas phase was continuously monitored with the NO_x
196 analyzer, while either the NO₂ CAPS or the LOPAP were coupled to the flow tube (**Fig. 3**). First, the
197 injector is placed at the downstream position of the reactor, ensuring no contact of the gas flow with
198 the v-dust coating. At this stage the background concentration levels for all instruments is recorded.
199 Afterwards, NO₂ is introduced in the reactor and a steady state concentration is achieved within a few
200 minutes. The NO levels are close to zero while a very low formation of HONO was observed,

201 probably due to hydrolysis of NO₂ on the wet Teflon lines (Finlayson-Pitts et al., 2003). This
202 contribution was taken into account for further calculations of the product yields. Thereafter, the
203 LOPAP was bypassed and the gas stream was driven through the NO₂ CAPS; as displayed in **Fig. 3**,
204 the NO₂ concentrations measured with the analyzer and the CAPS are in excellent agreement.
205 Subsequently, the injector is pulled out ($t = 0$ in **Fig. 3**) and the whole dust coating is exposed to the
206 gas flow. A fast consumption of NO₂ was observed due to NO₂ uptake on the volcanic sample, and a
207 gradual recovery to higher outlet concentrations was noticed. Simultaneously, NO was formed as a
208 product of the heterogeneous reaction. After achieving a steady state consumption of NO₂ and
209 formation of NO, the CAPS was bypassed to monitor the concomitant concentration of HONO with
210 the LOPAP for ca. 25 min. Then, the flow was sent back to the CAPS. The next step in the
211 experimental protocol was the irradiation of the surface with simulated sunlight; the initiated photo-
212 induced processes on the surface of the volcanic particles lead to an extra consumption of NO₂ and an
213 additional formation of NO. During the sample irradiation, the gas flow was sent to the LOPAP to
214 determine the HONO concentrations formed and then switched back to the CAPS. In the last step, the
215 injector is pushed back in, to control the NO₂ level. The steady state consumption of NO₂ and the
216 formation products such as NO and HONO under dark and simulated sunlight conditions, were used to
217 determine the corresponding uptake coefficients (γ_{ss}) and product yields.

218 2.4.2 Uptake coefficients and data analysis

219 The uptake coefficient of NO₂ on the v-dust surface can be derived from the following expression:

$$220 \quad \gamma_{\text{geom}} = \frac{2 \times k_{\text{kin}} \times r_{\text{tube}}}{C_{\text{NO}_2}} \quad (1)$$

221 where γ_{geom} is the geometric uptake coefficient, k_{kin} is the first order reaction rate loss of gas-phase
222 NO₂ (s⁻¹) in the kinetic regime, r_{tube} is the radius of the tube, and C_{NO_2} is the average molecular
223 velocity (cm/sec). Both the radius of the tube (0.49 cm) and the average molecular speed at 293 K are
224 known parameters, therefore only k_{kin} needs to be determined. Further information about the
225 calculations of uptake coefficients and diffusion corrections can be retrieved elsewhere (Romanias et
226 al., 2013, 2012; Tang et al., 2014) and are also given in Appendix A. Supplementary data.

227 The determination of the uptake coefficient using the geometric surface area (S_{geom}) can be considered
228 as an upper limit (Crowley et al., 2010). An alternative way for the calculation of the uptake
229 coefficient is using the specific surface area (A_s) of the solid, considering that all surface sites are
230 accessible to the gas phase molecules. For the determination of the Specific surface area (SSA), the
231 Brunauer-Emmett-Teller (BET) isotherm approach is applied and the corresponding uptake coefficient
232 (γ_{BET}) is given by the following expression:

$$233 \quad \gamma_{\text{BET}} = \frac{\gamma_{\text{geom}} \times S_{\text{geom}}}{S_{\text{BET}}} \quad (2)$$

234 where S_{BET} (m^2/g) is the product of the specific surface area (A_s) of the solid with the deposited mass
235 (g).

236 **3. Results and discussion**

237 **3.1 Determination of NO_2 uptake coefficients on v-dust samples**

238 This section includes the results of the kinetic measurements performed under simulated atmospheric
239 conditions aiming to determine the uptake coefficients of NO_2 on the volcanic samples. Initially, the
240 impact of experimental conditions on the uptake is discussed using dust from Hagavatn collection spot
241 as a model volcanic sample; this choice is based on two criteria. First, Hagavatn dust hot spot is in
242 close vicinity to Reykjavik - the most densely populated area in Iceland - and secondly, the air quality
243 in Reykjavik is very frequently impacted from massive loads of v-dust particles originating from
244 Hagavatndust hot spot. Therefore, it was considered as the most representative sample to study with
245 the ultimate objective to evaluate the corresponding impacts of NO_2 aged volcanic dust to the
246 chemistry of the local/regional atmosphere. Finally, at the end of this section a thorough comparison
247 between the uptake coefficients determined on the five volcanic samples under the same experimental
248 conditions is performed.

249 **3.1.1 Dependence of NO_2 uptake coefficient on the sample mass**

250 In this series of experiments, the steady state uptake coefficient was investigated as a function of
251 Hagavatn v-dust mass exposed to the NO_2 flow. The objective was to determine the v-dust surface
252 area involved in the interaction with NO_2 molecules. The experiments were performed under both dark

253 and simulated sunlight irradiation conditions ($j_{\text{NO}_2} = 4.5 \times 10^{-3} \text{ sec}^{-1}$) at temperature ($T = 293 \text{ K}$, 100
254 ppbV of NO_2 and dry conditions. The obtained results are presented in Appendix A **Fig. S3**. A linear
255 increase of the geometric uptake coefficient ($\gamma_{\text{ss,geom}}$) was observed as a function of the mass of
256 Hagavatr coated on the tube. This trend points out that the entire surface area of the solid sample is
257 accessible to NO_2 , and consequently, the BET specific surface area should be used for the
258 determination of the true uptake coefficient (Crowley et al., 2010). Furthermore, under UV light
259 conditions, the observed linear increase also indicates that the sample surface is homogeneously
260 irradiated, irrespectively of the sample mass (Herrmann, 2005). Similar trends were observed for the
261 remaining volcanic samples and have been also reported in literature for mineral oxides and natural
262 mineral dusts (El Zein et al., 2013a, 2013b; Romanias et al., 2016; Zein et al., 2014).

263 **3.1.2 Dependence of uptake coefficients on the irradiance intensity**

264 To evidence potential photocatalytic or photoinduced processes on the surface of the volcanic samples,
265 the irradiance intensity of the incident light was varied inside the reactor. The experiments were
266 carried out at 30% of RH, 293 K using 20 ppbV of NO_2 as inlet concentration and the steady-state
267 uptake coefficient was measured as a function of the number of UV lamps switched on, varying from
268 0 to 3 lamps. Appendix A **Fig. S4** displays the results on Hagavatr sample. A linear increase of the
269 uptake coefficient with the irradiance intensity was observed. It varied almost by a factor of 10
270 comparing the values under dark and 3 UV lamps, pointing out that NO_2 degradation rate is linearly
271 driven by the radian flux (Herrmann, 2005). However, if photons clearly induce specific
272 photoactivated phenomena on the v-dust surfaces it cannot be determined at this point whether they
273 are photocatalytic or photochemical. Nevertheless, similar trends have been noted in literature for
274 mineral oxides and natural mineral dusts (El Zein and Bedjanian, 2012; Tang et al., 2017; Zein et al.,
275 2014).

276 **3.1.3 Dependence of uptake coefficients on NO_2 concentration**

277 The dependence of the steady state uptake coefficient on the inlet concentration of NO_2 was studied in
278 the range of 20 to 140 ppbV. In this set of experiments Hagavatr volcanic sample was exposed to NO_2
279 at $T = 293 \text{ K}$, 30% of RH under both dark and UV irradiation conditions and the results are displayed
280 in **Fig. 4**. The simulated sunlight irradiation of the surface has promoted the uptake of NO_2 by a factor

281 of three in the entire concentration range. Furthermore, under both dark and light conditions, the
282 uptake coefficient was found to be almost constant for concentrations below 40 ppbV, however, above
283 that limit a slight decrease was observed; the latter may be attributed to the surface saturation by the
284 adsorbed intermediates. The solid lines of **Fig. 4** correspond to the empirical power fit of results
285 according to the following expressions:

$$286 \gamma_{ss,BET}(\text{dark}) = (3.9 \pm 1.2) \times 10^{-8} [\text{NO}_2]^{-0.53} \quad (3)$$

$$287 \gamma_{ss,BET}(\text{simulated sunlight}) = (2.5 \pm 0.8) \times 10^{-7} [\text{NO}_2]^{-0.73} \quad (4)$$

288 where $\gamma_{ss,BET}(\text{dark})$ and $\gamma_{ss,BET}(\text{simulated sunlight})$ refer to dark and simulated sunlight conditions,
289 respectively, and $[\text{NO}_2]$ (ppbV) is the initial concentration of NO_2 . The quoted uncertainties
290 correspond to the two sigma (2σ) precision of the fit of experimental results. Therefore, one can
291 extrapolate the uptake coefficient of NO_2 at any tropospheric concentration range.

292 3.1.4 Dependence of NO_2 uptake coefficient on RH

293 The uptake coefficients of NO_2 on Hagavatn sample were determined as a function of relative
294 humidity from dry conditions to 75% RH, the results are displayed in **Fig. 5**. Aiming to isolate the
295 effect of RH on the kinetic parameter, in this series of experiments the volcanic sample was always
296 exposed to 60 ppbV of NO_2 at 293 K. Under dark conditions, the steady state uptake coefficient was
297 found to be independent of RH in the whole investigated RH range. The solid black line in **Fig. 5**,
298 corresponds to the mean value of the steady state coefficient in the entire RH range:

$$299 \gamma_{ss,BET}(\text{dark}) = (3.6 \pm 0.2) \times 10^{-9} \quad (5)$$

300 the quoted uncertainties correspond to the 2σ precision of the fit of experimental results.

301 As shown in **Fig. 5**, the UV irradiation of the sample surface promoted the consumption of NO_2 in the
302 entire RH range compared to dark conditions; the $\gamma_{ss,BET}$ under simulated sunlight was promoted by a
303 factor of 3 compared to dark and was found to be independent of RH under ambient relative humidity
304 conditions i.e. RH higher than 10%. The dash black line in **Fig. 5**, corresponds to the mean value of
305 the steady state coefficient for ambient RH conditions:

306 $\gamma_{ss,BET}(\text{simulated sunlight}) = (9.4 \pm 0.5) \times 10^{-9}$ (6)

307 Interestingly, under dry conditions, the enhancement of $\gamma_{ss,BET}$ upon surface irradiation was by a factor
308 of 6.

309 The independent nature of $\gamma_{ss,BET}$ on RH does not preclude that water molecules do not affect the
310 reaction mechanism. More precisely, under UV light irradiation, H₂O is a well-known source of
311 radicals (i.e. $\cdot\text{OH}$, $\text{O}_2\cdot^-$) on mineral dust surfaces that contain photocatalysts (Chen et al., 2012;
312 Herrmann, 2005; Romanias et al., 2012; Schneider et al., 2014) and thus enhance the reactivity of the
313 surface towards NO₂ (Herrmann, 2005; Romanias et al., 2012; Zein et al., 2014). On the other hand,
314 adsorbed water may also block some sorptive and reactive sites and induce a decrease to $\gamma_{ss,BET}$
315 (Romanias et al., 2012, 2017; Zein et al., 2014). It seems that under ambient RH conditions (RH >
316 30%), the effect of sites blocking by water is probably compensated by its role as a source of radical
317 species on the surface of the dust. Under dark conditions, radical species are not expected to be
318 formed. However, the disproportionation of NO₂ can occur on the surface of the volcanic sample
319 leading to a continuous consumption of NO₂ (Finlayson-Pitts et al., 2003). Further details regarding
320 the reaction mechanism under both dark and light conditions versus relative humidity are given in
321 reaction mechanism section.

322 **3.1.5 Comparison of NO₂ uptake coefficients on various volcanic samples under defined** 323 **experimental conditions**

324 Aiming to compare the uptake coefficients of NO₂ on the different volcanic samples a series of
325 experiments were carried out under defined and atmospheric experimental conditions: 30% RH, NO₂
326 concentration 60 ppbV, under both dark and simulated sunlight. The results obtained are displayed in
327 **Fig. 6**, where for comparison purposes the international union of pure and applied chemistry, IUPAC
328 recommended value on mineral oxides is also displayed. A significant variation of the $\gamma_{ss,BET}$ as a
329 function of the origin of the samples can be noted. In addition, the simulated sunlight radiation of the
330 volcanic samples induced an increase to the $\gamma_{ss,BET}$ for all samples indicating the existence of photo-
331 induced processes on the surface of all dusts.

332 The dependence noted on the $\gamma_{ss,BET}$ values from one volcanic sample to another is significant. Despite
333 the fact that samples originate from close geographical regions, the chemical composition of the
334 magma that produced them is different (see SI materials) and thus variations in the composition of the
335 natural samples and contrasted surface properties are expected. Furthermore, taking into account that
336 their crystalline fraction is relatively low, ca. 20% for all samples beside Hagavatn, it makes any
337 correlation between mineralogical composition and reactivity challenging. The relative abundance of
338 elements could have been a base for comparison, however, it is quite similar for all samples, and no
339 relevant correlation trends were noticed.

340 Interestingly, a correlation between the uptake coefficients and the specific surface area was noticed
341 for both dark and light conditions (Appendix A **Fig. 5**); the highest the specific surface area, the
342 lowest the uptake coefficient. The latter could indicate that morphological parameters can play an
343 important role and affect the surface properties of the samples studied. It has been shown that the
344 specific surface area is inversely correlated with the particles size in literature (Ibrahim et al., 2018) –
345 and that small particles are more irregular. Moreover, it has been evidenced that the water monolayer
346 is formed at lower RH for natural mineral samples with small particle sizes due to higher OH group
347 surface density (Ibrahim et al., 2018; Tang et al., 2016). Therefore, a possible explanation could be
348 that the NO₂ uptake or/and the abundance of intermediate surface species formed are influenced by the
349 presence of surface OH group density.

350 The $\gamma_{ss, BET}$ values measured for the volcanic samples are in the same order of magnitude but relatively
351 lower than the IUPAC recommendation. However, it should be stressed out that the IUPAC
352 recommended value is based on studies performed with mineral oxides and not natural samples under
353 low pressure and dry conditions, although RH is a governing factor for NO₂ uptake. Recent studies
354 performed on oxides and natural or synthetic mineral dusts report uptake coefficients of NO₂ in the
355 order of 10⁻⁹ (Crowley et al., 2010; Li et al., 2010; Ndour et al., 2009), and thus similar or even lower
356 than those determine in the current study.

357 **3.2 Investigation of products formed along with NO₂ uptake**

358 The results presented in this section concern the determination of the gas-phase products of NO₂
359 interaction with the volcanic surfaces. The yield of the detected products (PY) was determined as the
360 ratio of the product concentration formed ($\Delta[\text{product}]$) to the concentration of NO₂ consumed
361 ($\Delta[\text{NO}_2]$) after achieving steady state conditions:

$$362 \text{ PY} = \Delta[\text{product}]/\Delta[\text{NO}_2] \quad (7)$$

363 To investigate the impact of experimental conditions, Hagavattn volcanic sample was used as model
364 volcanic sample. Finally, at the end of the section the product yields determined for all volcanic
365 samples under defined experimental conditions are presented and discussed.

366 **3.2.1 Product yield as a function of NO₂ initial concentration and relative humidity**

367 The impact of experimental conditions, such as NO₂ initial concentration (in the range of 40 to 140
368 ppbV) and relative humidity (from dry to 75% RH) on the yield of the products formed was
369 investigated at room temperature, under both dark and simulated sunlight, using Hagavattn as model
370 surface sample. In all cases, NO and HONO were measured as the only nitrogen containing gas phase
371 products. Regarding concentration dependence, the experiments were carried out at 30% of RH and
372 the yields of NO and HONO were $40\% \pm 10\%$ and $60\% \pm 10\%$, respectively, independent on NO₂
373 initial concentration. The product yield measurements as a function of RH were carried out at 60 ppbV
374 of initial NO₂. As displayed in **Fig. 7**, NO and HONO were detected as primary gas phase products,
375 with almost identical values under both dark and simulated sunlight conditions, however, their
376 formation was highly dependent on relative humidity. As relative humidity increases, the formation of
377 HONO is favored while that of NO is diminished. The latter is in accordance with the literature where
378 similar trends have been reported for mineral oxides (Baltrusaitis et al., 2009; Bedjanian and El Zein,
379 2012) and results seems to justify the mechanism proposed about enhanced formation of HONO on
380 humid surfaces (Finlayson-Pitts et al., 2003; Rodriguez et al., 2001). In addition, for RH above 20% a
381 nitrogen mass balance evidenced the complete conversion of adsorbed NO₂ to the gas phase products.
382 However, for RH below 10%, the nitrogen mass balance was not completed only considering the gas
383 phase products, thus the presence of nitrogen containing species on the surface, i.e. adsorbed NO₂ or

384 surface reaction products, is expected. The latter indicates that water plays a key role on the sorption
385 and/or reaction mechanism facilitating the transformation of NO₂ to gas phase products. Similar
386 formation yields and trend were noticed for the other volcanic samples and have been also reported in
387 literature on the surface of mineral oxides and natural desert dusts (Bedjanian and El Zein, 2012; Tang
388 et al., 2017).

389

390 **3.2.2 NO and HONO product yields on various volcanic samples under defined experimental** 391 **conditions**

392 In this series of experiments the volcanic samples were exposed to 60 ppbV concentration of NO₂,
393 30% of RH under both dark and simulated sunlight irradiation conditions. The results are presented in
394 **Table 1**. Considering the experimental uncertainties, no significant variation was noticed to the
395 formation yield of NO between the 5 volcanic samples under dark and simulated sunlight conditions
396 although significant differences were observed for the uptake coefficients. On the contrary, the HONO
397 formation yields for Eyjafjallajökull typical ash, Mýrdalssandur and Hagavatn, were systematically
398 higher than those measured for Dyngjusandur and Maelifellssandur v-dusts. Interestingly, it seems that
399 HONO formation in the gas phase is promoted on volcanic dusts with higher NO₂ uptake coefficients.

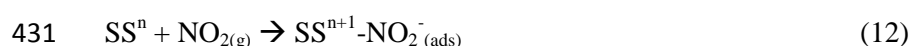
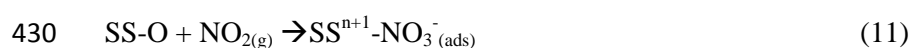
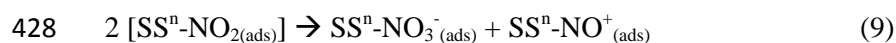
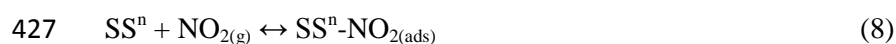
400 In addition, the irradiation of the surface increased the formation of NO for all samples while the
401 HONO yield was not influenced. The latter observation suggests that (i) either surface adsorbed
402 nitrogen species are photolysed or (ii) the surface is photoactivated and photocatalytic processes occur,
403 leading to the formation of NO. It should be noted that HONO photolysis in the gas phase is not
404 expected to occur in our system since the photolysis frequency of HONO is almost one order of
405 magnitude slower than NO₂, thus it is not expected to occur in our reactor, and HONO yields didn't
406 decrease upon surface irradiation. Concerning the total formation yields of gas phase products, under
407 surface irradiation a systematic increase was observed (except for typical ash sample) compared with
408 dark conditions, leading to an almost completion of the nitrogen mass balance for all samples within
409 the experimental uncertainties.

410 3.3 Proposed reaction mechanism

411 3.3.1 Dark conditions

412 The heterogeneous degradation of NO₂ on the surface of volcanic samples resulted in the formation of
413 both NO and HONO in the gas phase. Several pathways have been proposed to occur for the
414 transformation of NO₂ on mineral surfaces. In particular, NO₂ can be initially physisorbed on metal
415 sites (SSⁿ stands for surface site) of the mineral surface (Eq. (8)) and then disproportionate (Eq. (9)),
416 leading to the formation of surface nitrates (Eq. (9)) and gaseous NO (Eq. (10)) (Finlayson-Pitts et al.,
417 2003; Rodriguez et al., 2001). Furthermore, NO₂ can directly react with surface O atoms, SS-O, and
418 form surface nitrates (Eq. (11)) (Baltrusaitis et al., 2009). Alternatively NO₂ can be chemisorbed and
419 reduced to NO₂⁻ by metal sites, i.e. ferrous iron sites Fe²⁺, expected to be relatively abundant in the
420 volcanic samples, in an electron transfer reaction that is facilitated by adsorbed water (Eqs. (12) and
421 (13)) leading to HONO formation (Kebede et al., 2016). In the presence of water, the abundance of
422 surface OH groups increases, SS-OH (Ibrahim et al., 2018; Joshi et al., 2017; Tang et al., 2016), and
423 according to literature, NO₂ can form a hydrogen bond stabilized ONOOH species that could either
424 lead to the formation of gas HONO or isomerize and form adsorbed nitric acid (Eqs. (14) and (15))
425 (Baltrusaitis et al., 2009).

426



434 $SS-ONOOH \rightarrow SS-HNO_3$ (isomerization) (15)

435 The proposed reaction mechanism is in agreement with our experimental observations. Under dry
436 conditions, the dominant reaction pathways are: the disproportionation of NO_2 , leading to high
437 formation yields of $NO_{(g)}$ (Eqs. (8)-(10)); and reactions (11) and (12) respectively forming surface
438 nitrates and nitrites. Reactions (13)-(15) are still active pathways even under dry conditions, since the
439 removal of strongly adsorbed surface water requires a stronger thermal pretreatment method (> 500 K)
440 than the one followed in our study (Joshi et al., 2017). Consequently, the sequence of reactions
441 proposed seems to explain the high formation yields of NO, and the corresponding low HONO yields
442 observed for Hagavatn sample under dry conditions, as well as the absence of nitrogen mass balance
443 of the gas products due to the formation of surface adsorbed nitrogen containing species.

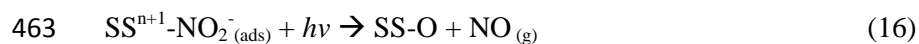
444 By increasing the relative humidity, the surface density of OH groups also increases considerably
445 (especially after water monolayer formation that is expected at RH greater than 25%-30% RH, (Joshi
446 et al., 2017), and thus reactions (13)-(15) which are competing to reactions (8), (9), (11) and (12) ,
447 become the dominant pathways leading to an enhanced formation of HONO. Consequently, the
448 formation of NO is diminished similar with the concentration of surface adsorbed species and a
449 nitrogen mass balance is observed.

450

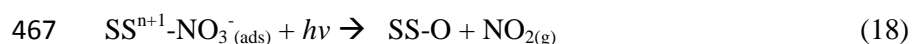
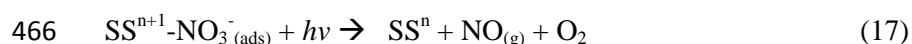
451 **3.2.2 UV light conditions**

452 Under simulated sunlight irradiation of the surface, and comparing the results obtained under fixed
453 experimental conditions (i.e. fixed NO_2 concentration and 30% RH - see **Table 1**) the uptake of NO_2
454 was enhanced, however unlike HONO the yield of NO was significantly influenced. These
455 observations could possibly point to the presence of photo-induced processes on the surface of
456 volcanic samples. Note that photocatalytic processes could also take place but considering that the
457 detailed mineralogical composition of the volcanic samples is not known and that samples are mostly
458 amorphous, the consideration of these processes is speculative and that they are not considered in the
459 proposed reaction mechanism.

460 The surface adsorbed nitrite species formed under dark conditions through reaction (12) could be
461 photolysed in presence of simulated sunlight ($h\nu$) producing gaseous NO and regenerating a SS-O
462 surface site according to reaction:



464 Similarly, nitrates formed through reaction (11) can be the source of gaseous NO and NO₂ through
465 reactions (17) and (18):



468 Reaction pathways (16)-(18) corroborate the photoinduced consumption of NO₂ under simulated
469 sunlight conditions, as well as the slight but systematic photoenhanced formation of NO observed on
470 volcanic samples under 30% of RH.

471 **4. Conclusions and atmospheric implications**

472 Within the framework of the current study, the reactivity of Icelandic volcanic samples towards NO₂
473 was studied as a function of several atmospheric parameters. Despite the relative close regions where
474 the samples were collected, the uptake coefficients varied significantly from one sample to another. It
475 is suggested that the origin of the magma and morphological differences between the samples could
476 possibly explain the variations noted. Besides the kinetics, the formation yields of NO and HONO
477 were also determined. The relative humidity was found to influence the balance between adsorbed and
478 gas phase products as well as the distribution of NO and HONO yields. Interestingly, under
479 atmospheric conditions (i.e. > 30% RH, ambient temperature) higher HONO formation yields were
480 noticed for the volcanic samples. Finally, based on the experimental observations of the current study,
481 a reaction mechanism was proposed.

482 Regarding the atmospheric implications, we estimate that the corresponding impacts of NO₂
483 transformation to HONO is expected to be significant in cases of volcanic eruptions or during more
484 frequent events such as volcanic dust storms. Indeed, using Iceland as a case study, it has been

485 evidenced that volcanic dust storms are much more frequent than volcanic eruptions transporting
486 volcanic aerosols to central Europe or Arctic (Dagsson-Waldhauserova et al., 2014a). Interestingly,
487 about half of these events occur in winter (dark season) when NO₂ concentrations in Reykjavik can
488 exceed 60 ppbV.

489 In an attempt to estimate the atmospheric significance of NO₂ heterogeneous degradation on volcanic
490 particles, the rate coefficient of NO₂ heterogeneous loss (k_{het} (hr⁻¹)) was calculated from the following
491 equation:

$$492 \quad k_{\text{het}} = \frac{\gamma \times c \times A}{4} \quad (19)$$

493
494 where, γ is the NO₂ uptake coefficient, c (cm/hr) is the mean molecular velocity, and A the aerosol
495 surface area density (cm²/cm³). Using Iceland as case study, under typical PM₁₀ concentrations during
496 a v-dust storm, i.e. ca. 300 µg/m³ (Arnalds et al., 2016, 2014; Dagsson-Waldhauserova et al., 2015;
497 Thorsteinsson et al., 2011), RH greater than 70%, NO₂ concentrations of ca 8 ppbV (annual average
498 values) (Hazenkamp-von Arx et al., 2004) and extrapolating the uptake coefficient of NO₂ under dark
499 conditions corresponding to winter season using Eq. (3), the heterogeneous loss of NO₂ is relatively
500 low (in the order of 10⁻⁶ hr⁻¹) and the estimated HONO formation rate is not expected to exceed 0.1
501 pptV/hr. Even considering the peak NO₂ concentration of 60 ppbV the HONO formation rate is below
502 0.3 pptV/hr. However, during severe dust events (7000 µg/m³), the heterogeneous loss of NO₂ could
503 be substantially higher (up to 10⁻⁴ hr⁻¹) and HONO formation rate could reach 4 pptV/hr. Considering
504 the severe dust event scenario during the summer season up to 10 pptV/hr of HONO can be expected
505 and thus a significant impact to the oxidative capacity of the regional atmosphere.

506 To conclude, the significance of NO₂ scavenging on the surface of volcanic particles is mainly
507 dependent on the v-dust atmospheric loads. Nevertheless, this study clearly evidences that volcanic
508 dust particles can efficiently uptake, scavenge and transform NO₂. Similar trends could be expected
509 for other pollutants. Indeed, in the recent study of Urupina et al. (2019) it was evidenced an efficient
510 uptake and transformation of sulfur dioxide to sulfates on these Icelandic volcanic dusts. Therefore,

511 Icelandic v-dust aerosols should be considered as reactive components of the atmosphere; In the
512 context of their long range transportation to Europe and especially Arctic it is expected to transport,
513 scavenge and transform pollutants and thus to alter the corresponding air quality and chemistry of the
514 atmosphere.

515 **Appendix A. Supplementary data**

516 Supplementary data associated with this article can be found in the online version at xxxxxx.

517

518 **Acknowledgments**

519 This work was achieved in the frame of Labex chemical and physical properties of the atmosphere
520 (Labex CaPPA) project, funded by agence nationale de la recherche (ANR) through the programme
521 d'investissements d'avenir (PIA) (No. ANR-11-LABX-0005-01), and contrat de plan état-région
522 changement climatique dynamique de l'atmosphère impacts sur la biodiversité et la santé humaine
523 (CPER CLIMIBIO) project, funded by the hauts-de-france regional council and the european regional
524 development fund (ERDF). Work of pavla dagsson-waldhauserova was partly funded by the czech
525 Science Foundation under the 'the role of high latitude dust in changing climate' (HLD-CHANGE)
526 project (Nr. 20-06168Y). Manolis N. Romanias is thankful to the INSU LEFE-CHAT program for
527 financial support.

528 **References**

- 529 Arnalds, O., Dagsson-Waldhauserova, P., Olafsson, H., 2016. The Icelandic volcanic aeolian
530 environment: Processes and impacts - A review. *Aeolian Res.* 20, 176-195.
- 531 Arnalds, O., Olafsson, H., Dagsson-Waldhauserova, P., 2014. Quantification of iron-rich volcanogenic
532 dust emissions and deposition over the ocean from Icelandic dust sources. *Biogeosciences* 11, 6623-
533 6632.
- 534 Arnalds, O., Thorarinsdottir, E F, Thorsson, J, Waldhauserova, P D, Agustsdottir, A M, 2013. An
535 extreme wind erosion event of the fresh Eyjafjallajökull 2010 volcanic ash. *Sci. Rep.* 3, 1257.
- 536 Auker, M R, Sparks, R S J, Siebert, L, Crossweller, H S, Ewert, J, 2013. A statistical analysis of the
537 global historical volcanic fatalities record. *J. Appl. Volcanol.* 2, 2.
- 538 Baltrusaitis, J, Jayaweera, P M, Grassian, V H, 2009. XPS study of nitrogen dioxide adsorption on
539 metal oxide particle surfaces under different environmental conditions. *Phys. Chem. Chem. Phys.* 11,
540 8295-8305.
- 541 Baratoux, D, Mangold, N, Arnalds, O, Bardintzeff, J-M, Platevoët, B, Grégoire, M, et al., 2011.
542 Volcanic sands of Iceland - Diverse origins of aeolian sand deposits revealed at Dyngjúsandur and
543 Lambahraun. *Earth Surf. Process.* 36,1789-1808.
- 544 Barnard, J C, Chapman, E G, Fast, J D, Schmelzer, J R, Slusser, J R, Shetter, R E, 2004. An evaluation
545 of the FAST-J photolysis algorithm for predicting nitrogen dioxide photolysis rates under clear and
546 cloudy sky conditions. *Atmos. Environ.* 38, 3393-3403.
- 547 Bedjanian, Y, El Zein, A, 2012. Interaction of NO₂ with TiO₂ surface under UV irradiation: Products
548 study. *J. Phys. Chem. A* 116, 1758-1764.
- 549 Bohn, B, Rohrer, F, Brauers, T, Wahner, A, 2005. Actinometric measurements of NO₂ photolysis
550 frequencies in the atmosphere simulation chamber SAPHIR. *Atmos. Chem. Phys.* 5, 493-503.
- 551 Boichu, M, Chiapello, I, Brogniez, C, Pere, J C, Thieuleux, F, Torres, B, et al., 2016. Current
552 challenges in modelling far-range air pollution induced by the 2014-2015 Baroarbunga fissure
553 eruption (Iceland). *Atmos. Chem. Phys.* 16, 10831-10845.
- 554 Butwin, M K, von Löwis, S, Pfeffer, M A, Thorsteinsson, T, 2019. The effects of volcanic eruptions
555 on the frequency of particulate matter suspension events in Iceland. *J. Aerosol Sci.* 128, 99-113.
- 556 Chen, H, Nanayakkara, C E, Grassian, V H, 2012. Titanium dioxide photocatalysis in atmospheric
557 chemistry. *Chem. Rev.* 112, 5919-5948.
- 558 Crowley, J N, Ammann, M, Cox, R A, Hynes, R G, Jenkin, M E, Mellouki, A, et al., 2010. Evaluated
559 kinetic and photochemical data for atmospheric chemistry: Volume V – heterogeneous reactions on
560 solid substrates. *Atmos. Chem. Phys.* 10, 9059-9223.
- 561 Dagsson-Waldhauserova, P, Arnalds, O, Olafsson, H, 2014a. Long-term variability of dust events in
562 Iceland (1949–2011). *Atmos. Chem. Phys.* 14, 13411-13422.
- 563 Dagsson-Waldhauserova, P, Arnalds, O, Olafsson, H, Skrabalova, L, Sigurdardottir, G M, Branis, M,
564 et al., 2014b. Physical properties of suspended dust during moist and low wind conditions in Iceland.
565 *Icel. Agric. Sci.* 27, 25-39.
- 566 Dagsson-Waldhauserova, P, Arnalds, O, Olafsson, H, Hladil, J, Skala, R, Navratil, T, et al., 2015.
567 Snow–Dust Storm: Unique case study from Iceland, March 6–7, 2013. *Aeolian Res.* 16, 69-74.
- 568 Dagsson-Waldhauserova, P, Magnúsdóttir, A O, Olafsson, H, Arnalds, O, 2016. The Spatial Variation
569 of Dust Particulate Matter Concentrations during Two Icelandic Dust Storms in 2015. *Atmosphere* 7.
- 570 Đorđević, D, Tošić, I, Sakan, S, Petrović, S, Đuričić-Milanković, J, Finger, D C, et al., 2019. Can
571 volcanic dust suspended from surface soil and deserts of Iceland be transferred to Central Balkan
572 similarly to African dust (Sahara)? *Front. Earth Sci.* 7.
- 573 El Zein, A, Bedjanian, Y, 2012. Interaction of NO₂ with TiO₂ surface under UV irradiation:
574 measurements of the uptake coefficient. *Atmos. Chem. Phys.* 12, 1013-1020.
- 575 El Zein, A, Bedjanian, Y, Romanias, M N, 2013a. Kinetics and products of HONO interaction with
576 TiO₂ surface under UV irradiation. *Atmos. Environ.* 67, 203-210.
- 577 El Zein, A, Romanias, M N, Bedjanian, Y, 2013b. Kinetics and products of heterogeneous reaction of
578 HONO with Fe₂O₃ and Arizona test dust. *Environ. Sci. Technol.* 47, 6325-6331.
- 579 Engelstaedter, S, Tegen, I, Washington, R, 2006. North African dust emissions and transport. *Earth-*
580 *Science Rev.* 79, 73-100.

581 Finlayson-Pitts, B J, Wingen, L M, Sumner, A L, Syomin, D, Ramazan, K A, 2003. The
582 heterogeneous hydrolysis of NO₂ in laboratory systems and in outdoor and indoor atmospheres: An
583 integrated mechanism. *Phys. Chem. Chem. Phys.* 5, 223-242.

584 George, C, Ammann, M, D'Anna, B, Donaldson, D J, Nizkorodov, S A, 2015. Heterogeneous
585 Photochemistry in the Atmosphere. *Chem. Rev.* 115, 4218-4258.

586 Gislason, S R, Hassenkam, T, Nedel, S, Bovet, N, Eiriksdottir, E S, Alfredsson, H A, et al., 2011.
587 Characterization of Eyjafjallajökull volcanic ash particles and a protocol for rapid risk assessment.
588 *Proc. Nat. Acad. Sci.* 108, 7307.

589 Groot Zwaftink, C D, Arnalds, Ó, Dagsson-Waldhauserova, P, Eckhardt, S, Prospero, J M, Stohl, A,
590 2017. Temporal and spatial variability of Icelandic dust emissions and atmospheric transport. *Atmos.*
591 *Chem. Phys.* 17, 10865-10878.

592 Gudmundsson, M T, Thordarson, T, Höskuldsson, Á, Larsen, G, Björnsson, H, Prata, F J, et al., 2012.
593 Ash generation and distribution from the April-May 2010 eruption of Eyjafjallajökull, Iceland. *Sci.*
594 *Rep.* 2, 572.

595 Hazenkamp-von Arx, M E, Götschi, T, Ackermann-Liebrich, U, Bono, R, Burney, P, Cyrus, J, et al.,
596 2004. PM_{2.5} and NO₂ assessment in 21 European study centres of ECRHS II: annual means and
597 seasonal differences. *Atmos. Environ.* 38, 1943-1953.

598 Herrmann, J M, 2005. Heterogeneous photocatalysis: state of the art and present applications. *Top.*
599 *Catal.* 34, 49-65.

600 Ibrahim, S, Romanias, M N, Alleman, L Y, Zeineddine, M N, Angeli, G K, Trikalitis, P N, et al.,
601 2018. Water interaction with mineral dust aerosol: Particle size and hygroscopic properties of dust.
602 *ACS Earth Space Chem.* 2, 376-386.

603 Ilyinskaya, E, Schmidt, A, Mather, T A, Pope, F D, Witham, C, Baxter, P, et al., 2017. Understanding
604 the environmental impacts of large fissure eruptions: Aerosol and gas emissions from the 2014–2015
605 Holuhraun eruption (Iceland). *Earth Planet. Sci. Lett.* 472, 309-322.

606 Joshi, N, Romanias, M N, Riffault, V, Thevenet, F, 2017. Investigating water adsorption onto natural
607 mineral dust particles: Linking DRIFTS experiments and BET theory. *Aeolian Res.* 27, 35-45.

608 Kebede, M A, Bish, D L, Losovyj, Y, Engelhard, M H, Raff, J D, 2016. The role of iron-bearing
609 minerals in NO₂ to HONO conversion on soil surfaces. *Environ. Sci. Technol.* 50, 8649-8660.

610 Kleffmann, J, 2007. Daytime Sources of Nitrous Acid (HONO) in the Atmospheric Boundary Layer.
611 *ChemPhysChem* 8, 1137-1144.

612 Lasne, J, Romanias, M N, Thevenet, F, 2018. Ozone Uptake by Clay Dusts under Environmental
613 Conditions. *ACS Earth Space Chem.* 2, 904-914.

614 Li, H J, Zhu, T, Zhao, D F, Zhang, Z F, Chen, Z M, 2010. Kinetics and mechanisms of heterogeneous
615 reaction of NO₂ on CaCO₃ surfaces under dry and wet conditions. *Atmos. Chem. Phys.* 10, 463-474.

616 Mellouki, A, Wallington, T J, Chen, J, 2015. Atmospheric chemistry of oxygenated volatile organic
617 compounds: Impacts on air quality and climate. *Chem. Rev.* 115, 3984-4014.

618 Moroni, B, Arnalds, O, Dagsson-Waldhauserová, P, Crocchianti, S, Vivani, R, Cappelletti, D, 2018.
619 Mineralogical and chemical records of Icelandic dust sources upon Ny-Ålesund (Svalbard Islands).
620 *Front. Earth Sci.* 6.

621 Nault, B A, Garland, C, Wooldridge, P J, Brune, W H, Campuzano-Jost, P, Crouse, J D, et al., 2016.
622 Observational constraints on the oxidation of NO_x in the upper troposphere. *J. Phys. Chem. A* 120,
623 1468-1478.

624 Ndour, M, Nicolas, M, D'Anna, B, Ka, O, George, C, 2009. Photoreactivity of NO₂ on mineral dusts
625 originating from different locations of the Sahara desert. *Phys. Chem. Chem. Phys.* 11, 1312-1319.

626 Ovadnevaite, J, Ceburnis, D, Plauskaite-Sukiene, K, Modini, R, Dupuy, R, Rimselyte, I, et al., 2009.
627 Volcanic sulphate and arctic dust plumes over the North Atlantic Ocean. *Atmos. Environ.* 43, 4968-
628 4974.

629 Perring, A E, Pusede, S E, Cohen, R C, 2013. An observational perspective on the atmospheric
630 impacts of alkyl and multifunctional nitrates on ozone and secondary organic aerosol. *Chem. Rev.*
631 113, 5848-5870.

632 Pfeffer, M A, Bergsson, B, Barsotti, S, Stefansdottir, G, Galle, B, Arellano, S, et al., 2018. Ground-
633 based measurements of the 2014-2015 Holuhraun volcanic cloud (Iceland). *Geosciences* 8.

634 Rodriguez, J A, Jirsak, T, Liu, G, Hrbek, J, Dvorak, J, Maiti, A, 2001. Chemistry of NO₂ on oxide
635 surfaces: Formation of NO₃ on TiO₂(110) and NO₂↔O vacancy interactions. *J. Am. Chem. Soc.* 123,
636 9597-9605.

637 Romanias, M N, Bedjanian, Y, Zaras, A M, Andrade-Eiroa, A, Shahla, R, Dagaut, P, et al., 2013.
638 Mineral oxides change the atmospheric reactivity of soot: NO₂ uptake under dark and UV irradiation
639 conditions. *J. Phys. Chem. A* 117, 12897-12911.

640 Romanias, M N, El Zein, A, Bedjanian, Y, 2012. Heterogeneous interaction of H₂O₂ with TiO₂ surface
641 under dark and UV light irradiation conditions. *J. Phys. Chem. A* 116, 8191-8200.

642 Romanias, M N, Zeineddine, M N, Gaudion, V, Lun, X, Thevenet, F, Riffault, V, 2016.
643 Heterogeneous interaction of isopropanol with natural Gobi dust. *Environ. Sci. Technol.* 50, 11714-
644 11722.

645 Romanias, M N, Zeineddine, M N, Riffault, V, Thevenet, F, 2017. Isoprene heterogeneous uptake and
646 reactivity on TiO₂: A kinetic and product study. *Int. J. Chem. Kinet.* 49, 773-788.

647 Romanías, M N, Ourrad, H, Thévenet, F, Riffault, V, 2016. Investigating the heterogeneous
648 interaction of VOCs with natural atmospheric particles: Adsorption of limonene and toluene on
649 Saharan mineral dusts. *J. Phys. Chem. A* 120, 1197-1212.

650 Romer, P S, Wooldridge, P J, Crouse, J D, Kim, M J, Wennberg, P O, Dibb, J E, et al., 2018.
651 Constraints on aerosol nitrate photolysis as a potential source of HONO and NO_x. *Environ. Sci.*
652 *Technol.* 52, 13738-13746.

653 Schneider, J, Matsuoka, M, Takeuchi, M, Zhang, J, Horiuchi, Y, Anpo, M, et al., 2014. Understanding
654 TiO₂ photocatalysis: Mechanisms and materials. *Chem. Rev.* 114, 9919-9986.

655 Tang, M, Cziczo, D J, Grassian, V H, 2016. Interactions of sater with mineral dust aerosol: Water
656 adsorption, hygroscopicity, cloud condensation, and ice nucleation. *Chem. Rev.* 116, 4205-4259.

657 Tang, M J, Cox, R A, Kalberer, M, 2014. Compilation and evaluation of gas phase diffusion
658 coefficients of reactive trace gases in the atmosphere: volume 1. Inorganic compounds. *Atmos. Chem.*
659 *Phys.* 14, 9233-9247.

660 Tang, M J, Huang, X, Lu, K D, Ge, M F, Li, Y J, Cheng, P, et al., 2017. Heterogeneous reactions of
661 mineral dust aerosol: implications for tropospheric oxidation capacity. *Atmos. Chem. Phys.* 17, 11727-
662 11777.

663 Thorsteinsson, T, Gísladóttir, G, Bullard, J, McTainsh, G, 2011. Dust storm contributions to airborne
664 particulate matter in Reykjavík, Iceland. *Atmos. Environ.* 45, 5924-5933.

665 Topaloglou, C, Kazadzis, S, Bais, A F, Blumthaler, M, Schallhart, B, Balis, D, 2005. NO₂ and HCHO
666 photolysis frequencies from irradiance measurements in Thessaloniki, Greece. *Atmos. Chem. Phys.* 5,
667 1645-1653.

668 Urupina, D, Lasne, J, Romanias, M N, Thiery, V, Dagsson-Waldhauserova, P, Thevenet, F, 2019.
669 Uptake and surface chemistry of SO₂ on natural volcanic dusts. *Atmos. Environ.* 217, 116942.

670 Vignelles, D, Roberts, T J, Carboni, E, Ilyinskaya, E, Pfeiffer, M, Dagsson Waldhauserova, P, et al.,
671 2016. Balloon-borne measurement of the aerosol size distribution from an Icelandic flood basalt
672 eruption. *Earth Planet. Sci. Lett.* 453, 252-259.

673 von Schneidmesser, E, Monks, P S, Allan, J D, Bruhwiler, L, Forster, P, Fowler, D, et al., 2015.
674 Chemistry and the linkages between air quality and climate change. *Chem. Rev.* 115, 3856-3897.

675 Wilson, T M, Cole, J W, Stewart, C, Cronin, S J, Johnston, D M, 2011. Ash storms: impacts of wind-
676 remobilised volcanic ash on rural communities and agriculture following the 1991 Hudson eruption,
677 southern Patagonia, Chile. *Bull. Volcanol.* 73, 223-239.

678 Zein, A E, Romanias, M N, Bedjanian, Y, 2014. Heterogeneous interaction of H₂O₂ with Arizona test
679 dust. *J. Phys. Chem. A* 118, 441-448.

680 Zeineddine, M N, Romanias, M N, Gaudion, V, Riffault, V, Thevenet, F, 2017. Heterogeneous
681 interaction of isoprene with natural Gobi dust. *ACS Earth Space Chem.* 1, 236-243.

682

683

684

685 **Tables.**

686 **Table 1:** Product yields of NO and HONO determined for the five volcanic samples under fixed
687 experimental conditions [NO₂] = 60ppbV and RH = 30% under dark and simulated sunlight radiation.

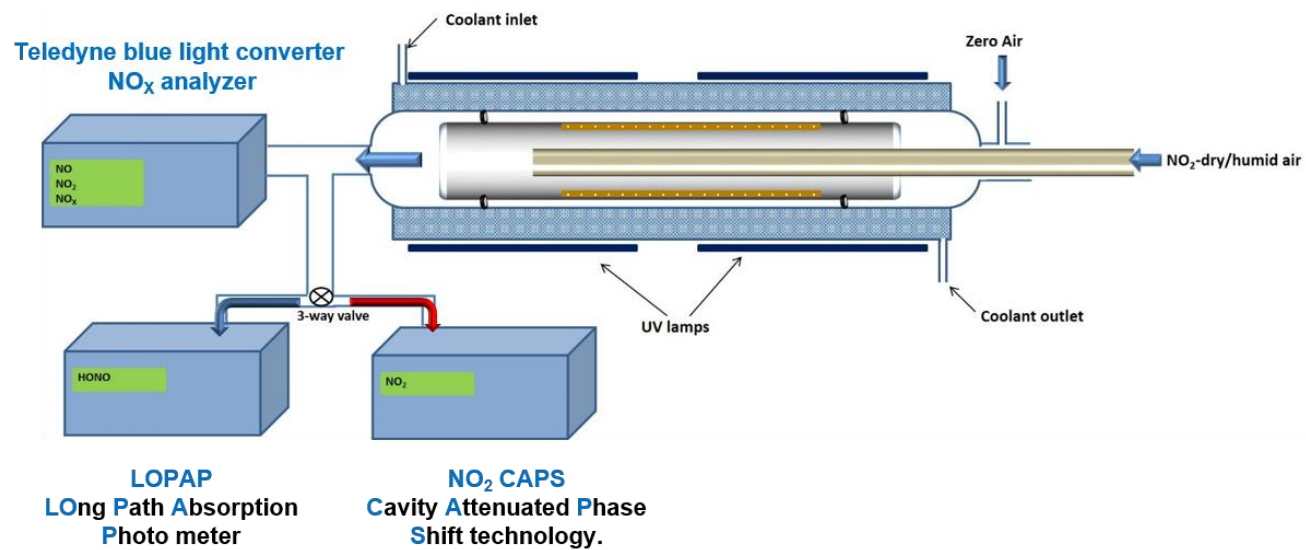
Volcanic sample	Yield NO		Yield HONO		Total yield	
	Dark	Light	Dark	Light	Dark	Light
Eyjafjallajökull typical ash	28%±4%	48%±7%	71%±11%	53%±8%	99%±15%	101%±15%
Mýrdalssandur	22%±3%	44%±7%	52%±8%	56%±8%	74%±11%	100%±15%
Hagavatn	37%±6%	45%±7%	60%±9%	62%±9%	97%±15%	107%±16%
Dyngjusandur	39%±6%	50%±8%	37%±6%	38%±6%	76%±11%	88%±13%
Maelifellssandur	28%±4%	37%±6%	48%±7%	47%±7%	76%±11%	84%±13%

688

689 **Figures**

690

691 **Fig. 1:** Schematic representation of the coated-wall flow-tube (CWFT) reactor used in this study. The
692 space filled with the coolant in between the two walls is shaded in blue. The volcanic sample coating
693 the inner surface of the Pyrex tube is shown in gray. The gas phase was monitored in real time with a
694 Nitrogen oxide (NO_x) analyzer, a long path absorption photometer (LOPAP) and occasionally with a
695 cavity attenuated phase shift (CAPS) NO_2 analyzer.

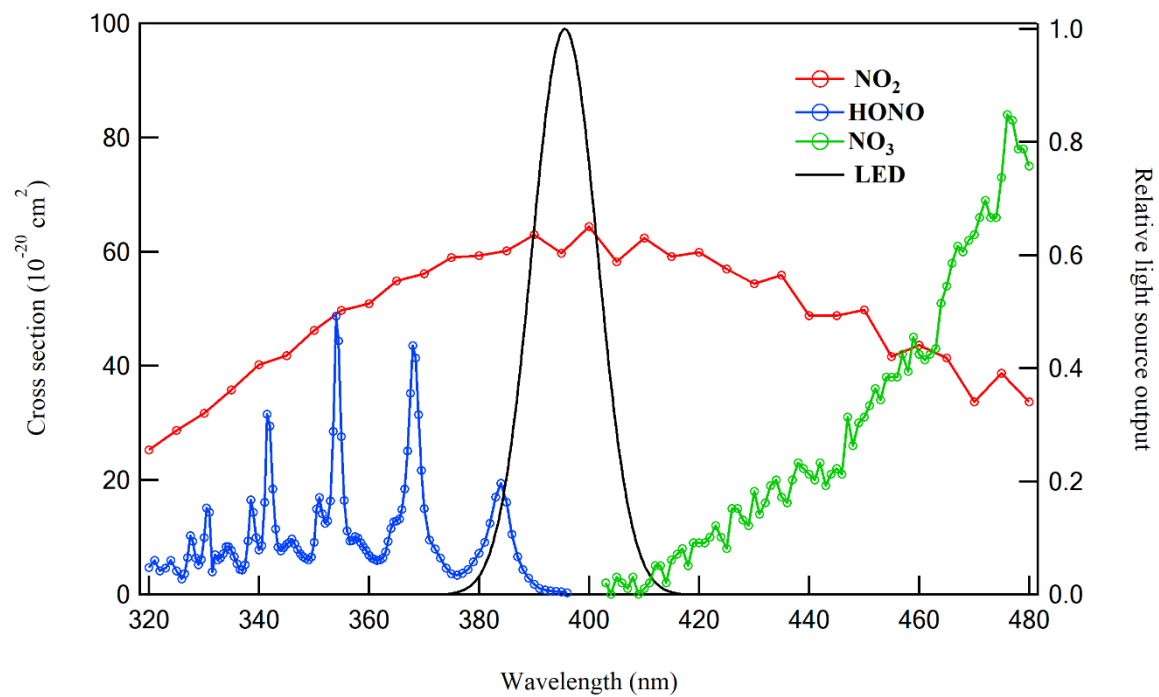


696

697

698

699 **Fig. 2:** Absorption spectra of NO₂ and possible interferences (HONO, NO₃) along with the spectral
700 output of the Light-emitting diode (LED) centered at 395 nm.



701

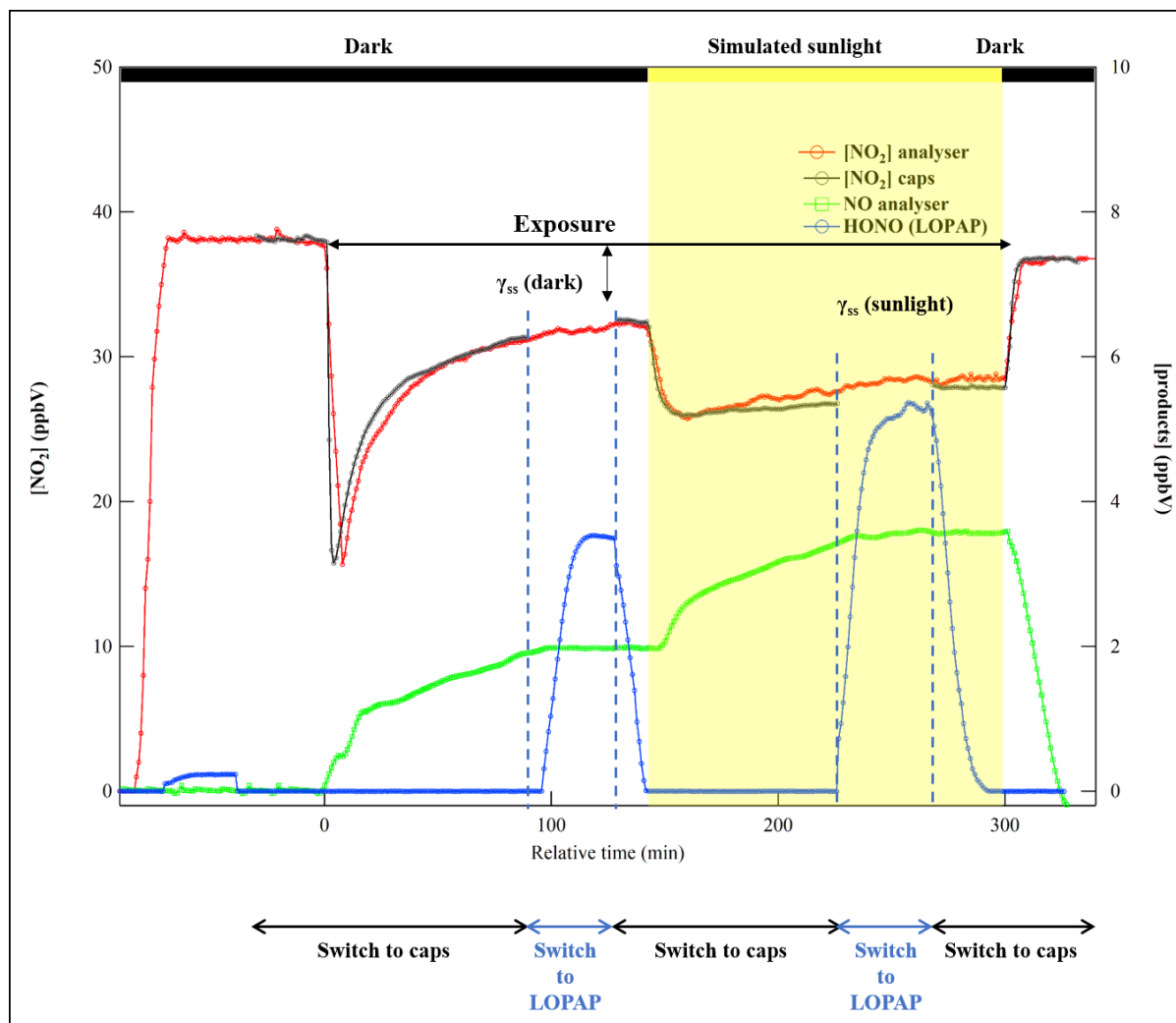
702

703

704

705 **Fig. 3:** Typical experiment of NO₂ adsorption/reaction on Hagavavn volcanic sample where all
 706 instruments were coupled with the flow tube reactor. Left vertical axis corresponds to the
 707 concentration profile of NO₂, [NO₂]. The concentrations profiles of NO and HONO, denoted as [NO]
 708 and [HONO], respectively, are also displayed (right vertical axis). $\gamma_{ss}(\text{dark})$ and $\gamma_{ss}(\text{sunlight})$ refer to
 709 the data averaged to determine the uptake coefficients under dark and simulated sunlight conditions,
 710 respectively.

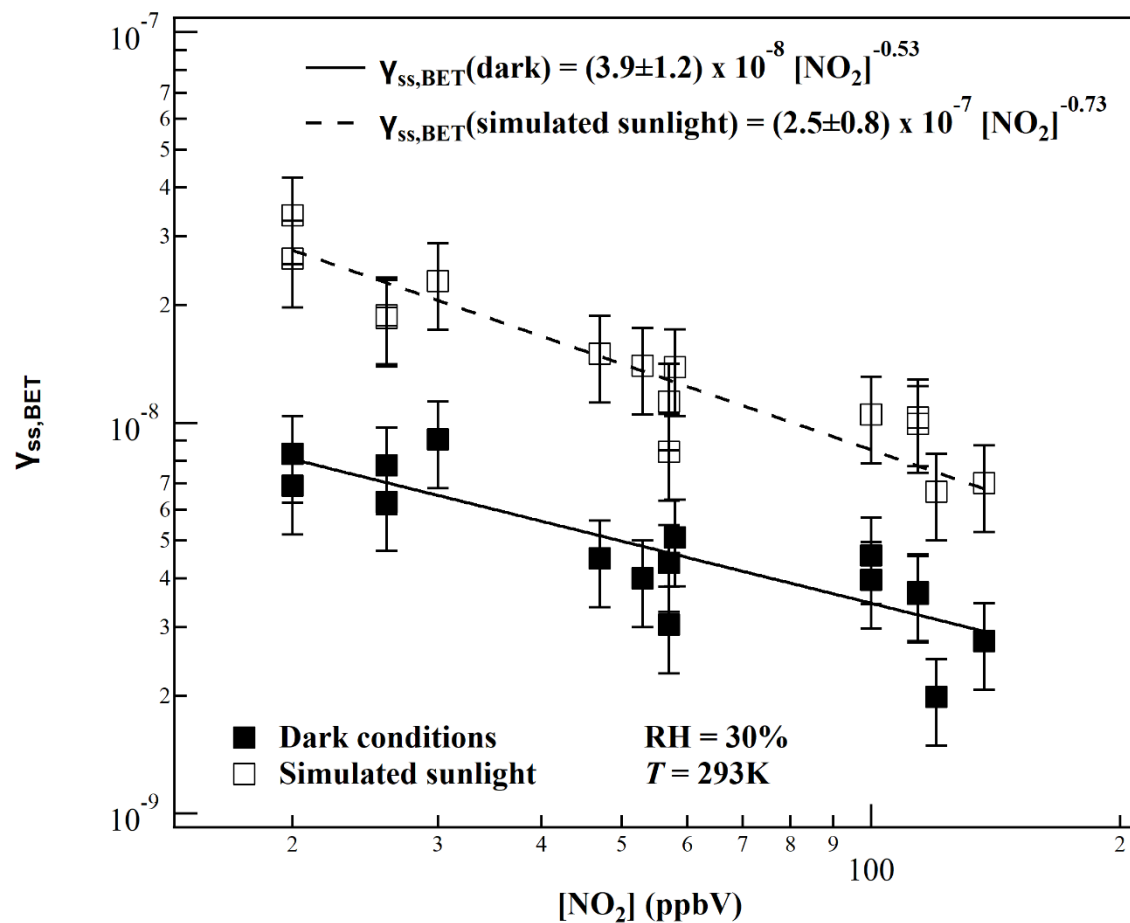
711



712

713

714 **Fig. 4:** Uptake coefficients of NO_2 ($\gamma_{\text{ss,BET}}$) on Hagavatr volcanic sample as a function of initial
 715 concentration under dark ($\gamma_{\text{ss,BET}}$ (dark)) and simulated sunlight irradiation ($\gamma_{\text{ss,BET}}$ (simulated
 716 sunlight)). Error bars denote the overall uncertainty on $\gamma_{\text{ss,BET}}$ determination (ca. 25%) that arise mostly
 717 from the determination of Specific surface area (SSA). The solid and dashed lines corresponds to the
 718 fit of experimental data using an empirical power function, under dark and simulated sunlight
 719 radiation respectively. Temperature was set at $T = 293$ K, and relative humidity, $\text{RH} = 30\%$

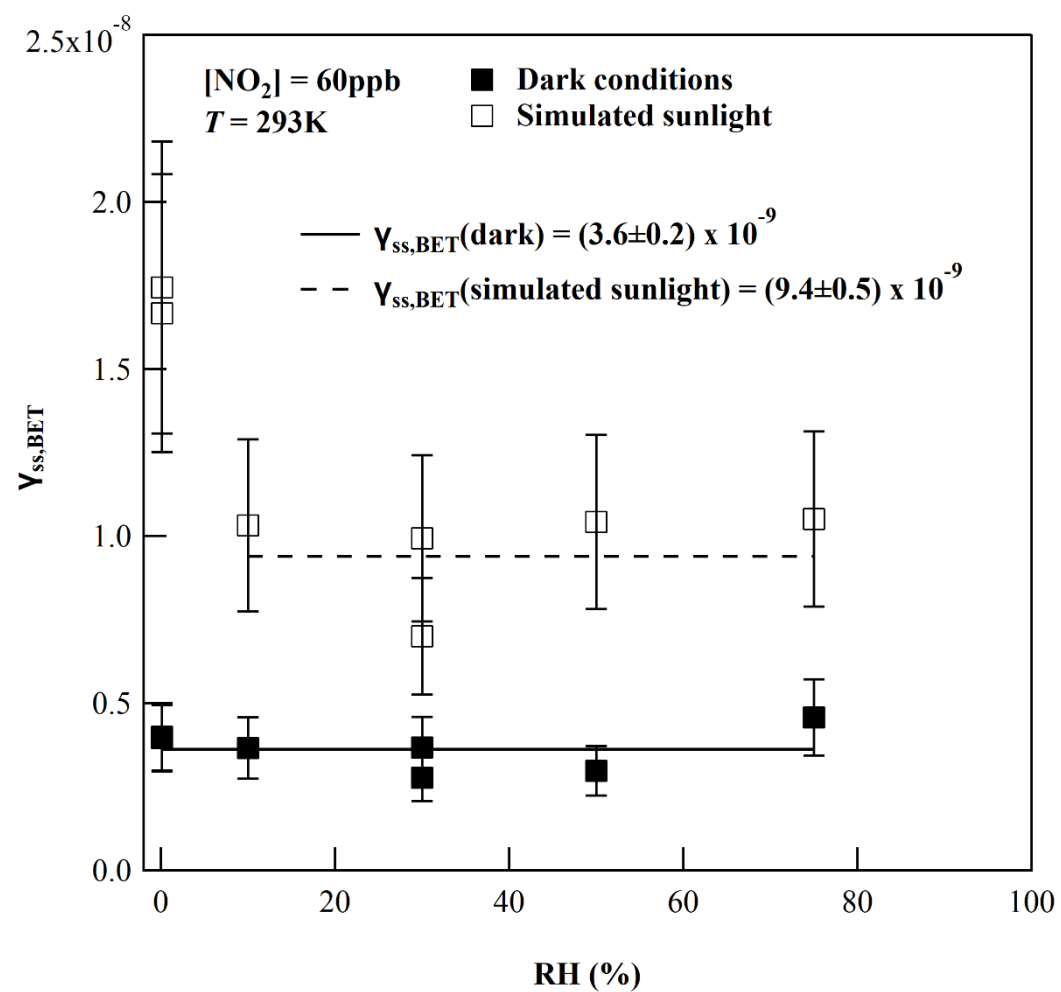


720

721

722

723 **Fig. 5:** Uptake coefficients of NO₂ on Hagavatr volcanic sample as a function of relative humidity
 724 under dark and simulated sunlight irradiation. Error bars reflect the overall uncertainty on $\gamma_{ss,BET}$
 725 determination (ca. 25%) that arise mostly from the determination of SSA. The solid and dashed lines
 726 correspond to the average value of the $\gamma_{ss,BET}$.

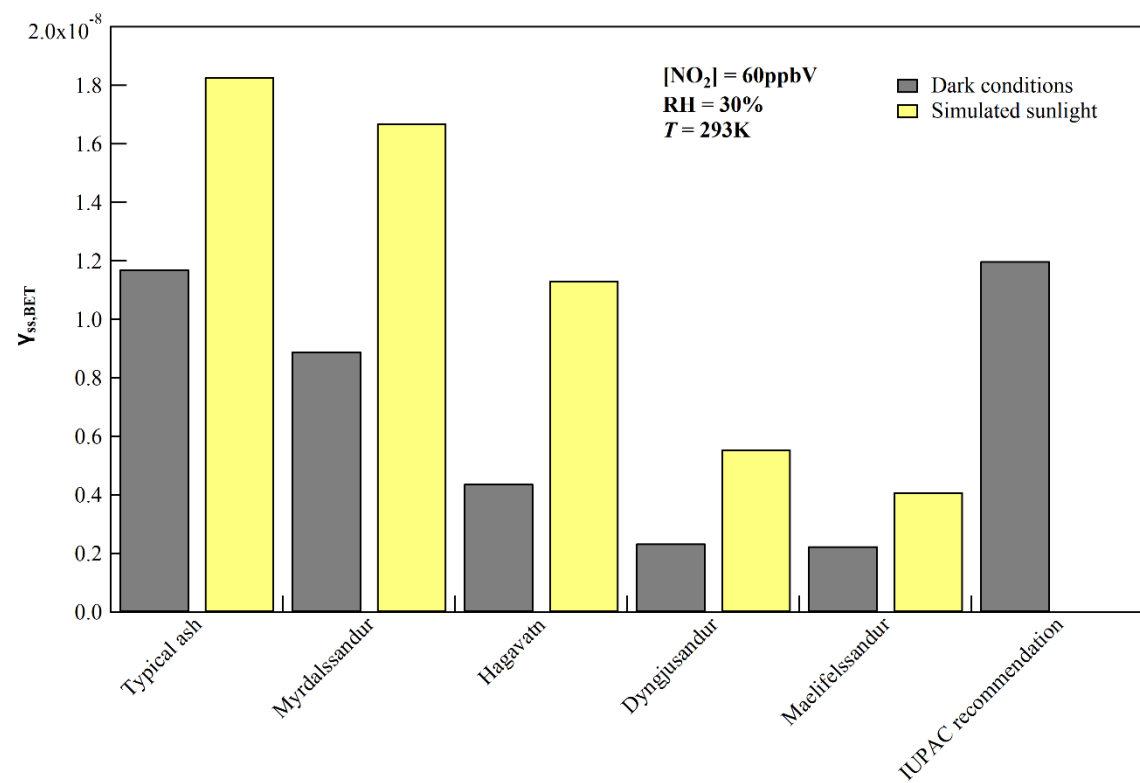


727

728

729

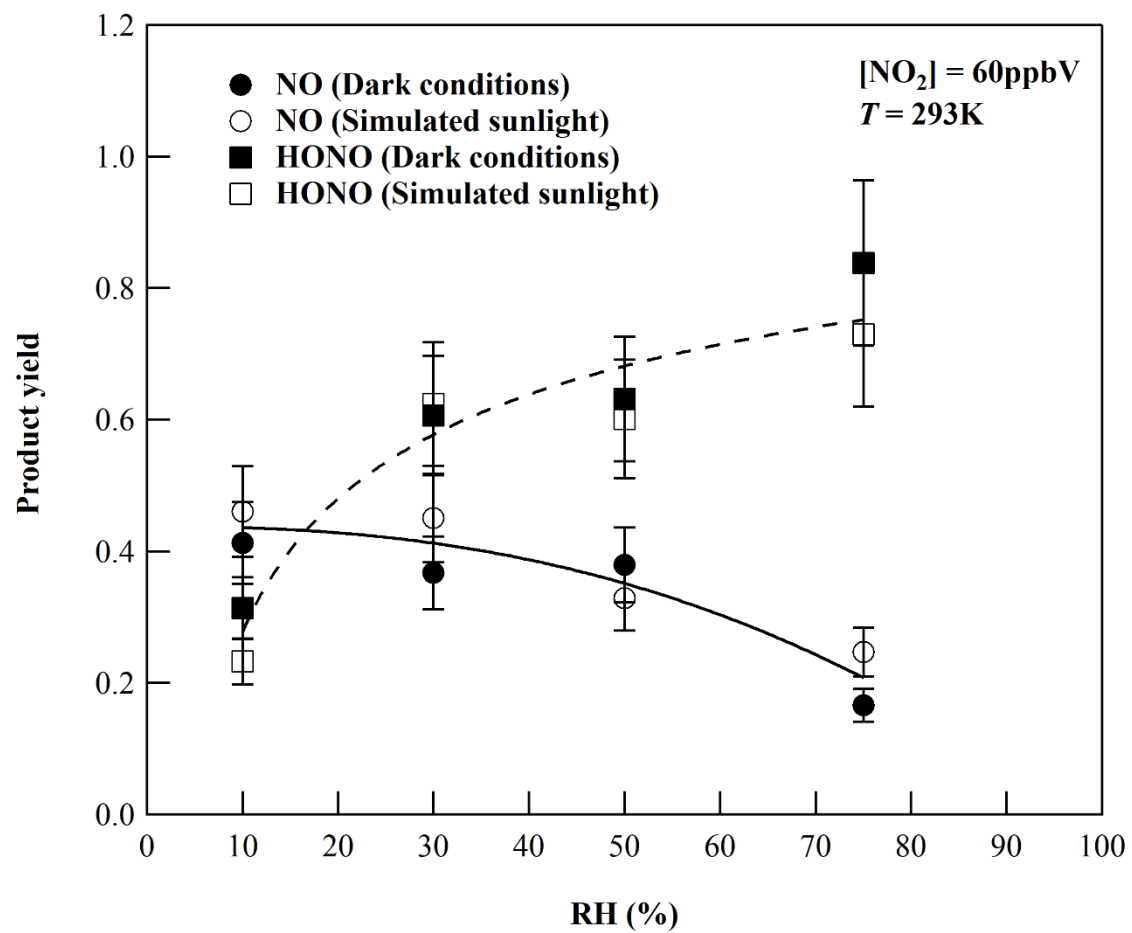
730 **Fig. 6:** Uptake coefficients of NO_2 as a function of volcanic samples origin under dark and simulated
731 sunlight irradiation. For comparison purposes, the recommended uptake coefficient value proposed by
732 the international union of pure and applied chemistry (IUPAC) panel for mineral oxides under dark
733 and dry conditions is given.



734

735

736 **Fig. 7:** Product yields of NO (circles) and HONO (squares) formation determined as a function of
737 relative humidity upon reaction of NO₂ with Hagavtn volcanic sample under dark and simulated
738 sunlight radiation. Error bars reflect the overall uncertainty on the product yields (ca. 15%). The solid
739 and dashed lines are the empirical fit of experimental results (both dark and simulated sunlight) to
740 demonstrate the corresponding trends of NO and HONO yields versus RH.



741